This article has been accepted for publication in IEEE Access. This is the author's version which has not been fully edited and content may change prior to final publication. Citation information: DOI 10.1109/ACCESS.2024.3400623

IEEE Access
Multidisciplinary ⋮ Rapid Review ⋮ Open Access Journal

Date of publication xxxx 00, 0000, date of current version xxxx 00, 0000.

Digital Object Identifier 10.1109/ACCESS.2017.DOI

DAT-based Formation Control with Different Scale Factor of Relative Information Measurement

CHENG FU[1], ERHAN WANG[1], XIUCHUAN HUANG[2], QIN YANG[1], ZHEYU LI[1], WEI SHANG[1,3,4]

[1]School of Mechanical Engineering, Hubei University of Technology, Wuhan 430068, China
[2]Wuhan Railway Vocational and technical College, Wuhan 430205, China
[3]Ningbo University, Zhejiang 315211, China
[4]Ningbo Cixing Co.,Ltd., Ningbo 315000, China

Corresponding author: XiuChuan Huang (20070498@wru.edu.cn).

ABSTRACT This paper proposes an unmanned surface vehicles (USVs) formation control method based on distributed average tracking (DAT) with different relative information measurement scale factors. Firstly, the DAT algorithm is designed in the controller to control the time when the system reaches stability. Then, the relative position information of adjacent USVs is measured by installing distance sensors and direction sensors on each USV, and different scale factors are used to control the formation of USVs, and improve the stability and robustness of its control system. Finally, the effectiveness of the method proposed in this paper is verified by numerical simulation experiments.

INDEX TERMS DAT, different scale factor, information measurement

I. INTRODUCTION

Science and technology are developing rapidly, and the field of autonomous driving is also maturing. USVs are coming into researchers' view. Due to the limitations of a single USV operation, the formation control of USVs has become a hotspot in future research due to the superiority of its intelligence, large scale, high efficiency, and high fault tolerance [1]–[3]. The arrival of the era of USV is only a matter of time [4]. At the same time, due to the diversity and complexity of their tasks, and the uncertainty of their operating environment, they also face many difficulties, where the low precision and poor robustness of formation control are urgent to solve.

Many researchers have studied this problem. To strengthen the robustness of USV formation control, Mu et al. used adaptive technology [5]. Gu et al. distributed time-varying formation guidance and developed the surge speed and yaw rate control laws [6].Bases on an extended-stateobserver-based, Lv et al. proposed a distributed model predictive control model [7]. Huang developed a bounded-feedback adaptive law [8]. In reference [9], the trajectory communication systems and policy-sharing mechanisms were designed to improve the obstacle avoidance ability of USV with leader-follower method. For the problem of significant tracking errors, Fu H. et al. created the formation controller by applying the virtual leader strategy [10].An et al. proposed a non-event-triggered reference governor for adaptive adjustment of transient tracking errors [11]. Dong et al. proposed a virtual transition trajectory to guide the design of the tracking controller, which allowed the tracking error to be concurrent tiny [12]. To ensure the boundedness of all signals of the closed-loop system and attain the performance index within formation errors, the high-gain observer was used to rebuild the velocity of its leader, and a singularity-free formation controller was designed [13]. For the problem of limited time distributed formation control problem of USV, Huang et al. propose two USV formation control structure architectures to achieve finite-time convergence based on an adaptive algorithm [14]. Dai et al. proposed an adaptive cluster control to ensure the internal stability of a closed-loop system with a predetermined performance [15].Yang et al. propose an adaptive compensation mechanism to improve the fault tolerance of multi-agent systems [16]. Pan et al. propose a predefined- time adaptive neural control method for MASs that enables the followers to accurately track the desired trajectory with predefined time [17].However, in reference [5]–[8], the modelling scheme of the proposed controller is complicated with low computational efficiency. Moreover, in reference [9]–[14], the desired convergence velocity cannot be controlled during convergence.

This work is licensed under a Creative Commons Attribution-NonCommercial-NoDerivatives 4.0 License. For more information, see https://creativecommons.org/licenses/by-nc-nd/4

This article has been accepted for publication in IEEE Access. This is the author's version which has not been fully edited and content may change prior to final publication. Citation information: DOI 10.1109/ACCESS.2024.3400623

However, the formation of USVs usually completes some advanced tasks through collaboration, such as maritime search and rescue [18] and ocean survey [19], [20], which also requires higher control accuracy and robustness. If the convergence velocity differs from the expectation, rescue delay and investigation errors may be caused, resulting in many human and material losses. DAT is an algorithm in which multiple agents cooperate to achieve control objectives. In reference [21], the DAT algorithm is robust to initialization errors and can deal with the bounded input signal, input velocity, and input acceleration is proved. Liu et al proposed a hierarchical average-tracking algorithm, obtaining the consensus convergence conditions for the agents with the directed and balanced topology [22]; In reference [23], in the case of selecting the proper control gain, the state of multiagent can converge to the average value of bounded derivative is proved through DAT algorithm. In reference [24], a discontinuous control algorithm is proposed to solve the distributed moderate tracking problem of reference signals with bounded acceleration to ensure the target position is reached in a finite time. Hong et al. also investigated the distributed average tracking problem of the disturbed second-order multiagent systems so that each agent can accurately track the average of multiple time-varying signals in a finite time, even in the absence of time measurement [25]. Many researches have shown that the DAT algorithm can control the convergence rate of the agent and make it converge to the expected value in a limited time. However, the above research did not consider the scale factor of the distance sensor of adjacent USVs. In this case, the measured relative position information could not meet the given relationship, resulting in low stability and poor robustness of formation control [26], [27]. Therefore, solving the problem of USV formation control under different scale factors is necessary.

This paper proposes the formation control of USVs based on the DAT algorithm with different relative information measurement scale factors. First, the DAT algorithm is designed in the controller, which can control the time the USVs formation reach stability. Then, each USV is equipped with distance and direction sensors to measure the relative positions of neighbours [28], [29], and the formation of USVs is controlled with different scale factors to improve the stability and robustness of its formation control. Finally, the effectiveness of the proposed control scheme is verified by simulation.

In summary, the contributions of this paper are as follows:

1) Compared with the reference [10]–[15], the DAT algorithm proposed in this paper has a broader application range and requires less computation, because there is no additional updating rule for gain setting. For the bounded deviation of the acceleration reference, the error can reach the limit range in a finite time, the final boundary and the finite convergence time can control the gain used. Moreover, when the error of the convergent acceleration reference goes to zero, the gain can be adjusted to achieve the desired convergence rate and predetermined time convergence, improving the accuracy of formation control.
2) Considering the different scale factors of distance sensors of adjacent USVs, a new relationship is established to solve the problem of poor robustness of USV formation.

The rest of this paper is shown as follows. Section 2 demonstrates the dynamic model of the USV and the main control objectives. Section 3 illustrates the stability proof of the proposed control scheme. Section 4 carries out the simulation experiment to demonstrate the effectiveness of the control scheme in this paper. Section 5 summarizes the conclusion of this paper.

II. PROBLEM STATEMENTS

A. PREPARATORY KNOWLEDGE

Assume that a USVs formation consists of N USVs, and orders node pairs $(\upsilon_N, \varepsilon_N)$ represent a directed graph, where $\upsilon_N := \{1, 2, ..., N\}$, edge set $\varepsilon_N \subseteq (\nu_N \times \nu_N)$. If the j node can obtain the information of the i node, j is the neighbor of i. Corresponding to $(\upsilon_N, \varepsilon_N)$, the adjacency matrix $d := [a_{ij}] \in \mathbb{R}^{N\times N}$, and the Laplacian matrix $\varphi := [l_{ij}] \in \mathbb{R}^{N\times N}$ are defined as $a_{ij} \begin{cases} > 0 \text{ if } j \in N_i \\ = 0 \text{ otherwise} \end{cases}$ and $l_{ij} = \begin{cases} \sum_{j\in N_i} a_{ij}, \text{for } i = j, \\ -a_{ij}, \text{ otherwise,} \end{cases}$, where N_i is the set of the neighbours of ith node. The directed path of a directed graph consists of a series of edges connecting its continuous nodes. If at least one direct path connects the node pair $\{i, j\}, \forall i, j \in V$, the directed graph g is defined as strongly-connected. If g is strongly-connected, φ has a simple eigenvalue 0 and the corresponding positive left eigenvector of φ is

$$w_1 = w := [\omega_1, ..., \omega_N]^T \in \mathbb{R}^N$$

and $w_r \in span\{1_N\}$ is a right eigenvector, so $\omega_i \in \mathbb{R}^+, \forall_i = 1, 2, ..., N$ with ${w_1}^T w_r = 1$ can be obtained. Hence, $\varphi 1_N = O_N$ and $w^T\varphi = O_N^T$. For a weight-balanced directed graph, $\sum_{j=1}^{N} a_{ij} = \sum_{j=1}^{N} a_{ji}, \forall_i = 1, ..., N$, and $w \in span\{1_N\}$. For a weight-unbalanced graph, $\sum_{j=1}^{N} a_{ij} = \sum_{j=1}^{N} a_{ji}$ does not satisfy $i = 1, 2, ..., N$.

B. DYNAMIC MODEL OF USVS

This section introduces the dynamic model of USV. The motion of the USV in three-dimensional space is a compound motion consisting of a straight motion along three axes and a rotational motion around three axes, including transverse and longitudinal oscillations of the X-axis, transverse and longitudinal oscillations of the Y-axis, vertical and bow oscillations along the z-axis. Since the USV research in this paper mainly navigates on river surfaces, the effects of heave, pitch and roll can be ignored. Therefore, the model is simplified into a nonlinear model of three degrees of freedom (DOF).

This work is licensed under a Creative Commons Attribution-NonCommercial-NoDerivatives 4.0 License. For more information, see https://creativecommons.org/licenses/by-nc-nd/4

This article has been accepted for publication in IEEE Access. This is the author's version which has not been fully edited and content may change prior to final publication. Citation information: DOI 10.1109/ACCESS.2024.3400623

The double integrator designs the two models, and the actual signal model is shown as follows: Actual signal model

$$\begin{cases} \dot{\eta} = J(\eta)v \\ M\dot{v} + Cv + Dv = \tau \end{cases} \tag{1}$$

where η, v, τ are the measured actual position, velocity and acceleration of the USV, respectively. $M = \begin{bmatrix} m_{11} & 0 & 0 \\ 0 & m_{22} & m_{23} \\ 0 & m_{32} & m_{33} \end{bmatrix}$ is the Inertial matrix in inertial coordinate system, $C = \begin{bmatrix} 0 & 0 & -m_{22}v - m_{23}r \\ 0 & 0 & m_{11}u \\ m_{22}v + m_{23}r & -m_{11}u & 0 \end{bmatrix}$ is Coriolis and the centripetal force matrix, and $D = \begin{bmatrix} d_{11} & 0 & 0 \\ 0 & d_{22} & d_{23} \\ 0 & d_{32} & d_{33} \end{bmatrix}$ is the Hydrodynamic damping matrix. $J(\eta) = \begin{bmatrix} \cos\varphi & -\sin\varphi & 0 \\ \sin\varphi & \cos\varphi & 0 \\ 0 & 0 & 1 \end{bmatrix}$ is the coordinate system transformation matrix $\tau = [\tau_1, \tau_2, \tau_3]^T$. τ_1, τ_2, τ_3 represent the forward, transverse drift force and yawing moment respectively.They are the control input vectors of the design.

Suppose there is a time-varying reference for each USV, and assume that each USV only knows its references. Each reference signals satisfies the reference signal model, which is described as follows:

$$\begin{cases} \dot{p} = J(p)q \\ M\dot{q} + Cq + Dq = r \end{cases} \tag{2}$$

The position vector $\eta = \begin{bmatrix} x & y & \varphi \end{bmatrix}^T$ of the USV is composed of the actual position (x, y) and yaw angle φ in the inertial coordinate system, and the velocity vector $v = [u, v, r]^T$ is composed of forward velocity u, transverse drift velocity v and angular velocity t. Where $p = \begin{bmatrix} a & b & c \end{bmatrix}^T$, $q = \begin{bmatrix} m & n & o \end{bmatrix}^T, t = \begin{bmatrix} r_1 & r_2 & r_3 \end{bmatrix}^T$, respectively are the assumed reference position, velocity and acceleration. r_1, r_2, r_3 represent the reference forward, transverse drift force and yawing moment, respectively. Assume that each USV has a time-varying reference.

Remark 1: Make $\mathbb{R}^N$ and $\mathbb{C}^N$ be the set of real and complex vectors of order N, and the set of real matrices of size $N \times M$ is $\mathbb{R}^{N\times M}$. $\mathbb{R}^+$ is denoted as the set of positive real numbers, and $1_N \triangleq [1, ...1]^T, 0_N \triangleq [0, ..., 0]^T \in \mathbb{R}^N$. I_N expresses the Nth order identity matrix and the square matrix $\hat{0}_N \in \mathbb{R}^{N\times N}$ has all zero elements. For $p = \{1, 2, ..., \infty\}$, the p-norm of a real-valued vector or matrix is represented as $\| \cdot \|_p$.

C. ERROR DESIGN

In this section, the error in this paper is designed. Let the wrong variables $e_1 = D_x\eta_i - \bar{p}, e_2 = v_i - \bar{q}, e_3 = \phi_i$, taking the derivative of them yields:

$$\begin{cases} \dot{e}_{1i} = D_x e_{2i} + D_x\bar{q} - \bar{q} \\ \dot{e}_{2i} = -\mu_2 e_{3i} - 2\mu_1 e_{1i} + 2\mu_1\delta_{1i} + \tilde{r}_i \\ \dot{e}_{3i} = -\mu_2 e_{3i} - \mu_1 e_{1i} + \mu_1\delta_{1i} \end{cases} \tag{3}$$

where $\tilde{r}_i = r_i - \bar{r}$, by using the vector notations $e_k = [e_{k1}, \cdots, e_{kN}]^T \in R^N$ for $e_k = [e_{k1}, \cdots, e_{kN}]^T \in R^N$ and $E = [e_1^T, e_2^T, e_3^T]^T$, we can get:

$$\begin{cases} \dot{e}_1 = D_x e_2 + D_x\bar{q} - \bar{q} \\ \dot{e}_2 = -\mu_2 e_3 - 2\mu_1 e_1 + 2\mu_1\delta_1 + \tilde{r} \\ \dot{e}_3 = -\mu_2 e_3 - \mu_1 e_1 + \mu_1\delta_1 \end{cases} \tag{4}$$

where $A_2 = \begin{bmatrix} 0 & D_x & 0 \\ -2\mu_1 & 0 & -\mu_2 \\ -\mu_1 & 0 & -\mu_2 \end{bmatrix} \otimes I_N$

$B_2 = \begin{bmatrix} 0 & 0 \\ 2\mu_1 & 1 \\ \mu_1 & 0 \end{bmatrix} \otimes I_N$

$C_2 = \begin{bmatrix} D_x & -1 \\ 0 & 0 \\ 0 & 0 \end{bmatrix} \otimes I_N$. $\otimes$ is Kronecker product.

In addition, the equation (4) can be written as $\dot{E} = A_2E + B_2\begin{bmatrix} \delta_1 \\ \tilde{r} \end{bmatrix} + \bar{q}C_2$

D. DAT ALGORITHM

1) Distributed Averaging Filter

In this part, a distributed average filter of the DAT algorithm is proposed, Fig. 1 is a block diagram of the proposed DAT algorithm to illustrate the filter and controller of agent i. The update rule of the filter is defined as

$$\begin{aligned} \dot{\xi}_{1i} &= \xi_{2i} - k_1\omega_i \sum\nolimits_{j\in N_i} a_{ij}(\xi_{1i} - \xi_{1j}) \\ \dot{\xi}_{2i} &= -k_2\omega_i \sum\nolimits_{j\in N_i} a_{ij}(\xi_{2i} - \xi_{2j}) + r_i \end{aligned} \tag{5}$$

where $a_{ij} > 0$ for $j \in N$, if $a_{ij} = 0, j \notin N$. $\xi_1, \xi_2 \in R$ are the condition of the filter, k_1, k_2 are the control gain and ω_i is the ith element of ω that is estimated offline.

Define $p \triangleq [p_1, \cdots, p_N]^T$, $q \triangleq [q_1, \cdots, q_N]^T$, $r \triangleq [r_1, \cdots, r_N]^T$, $\xi_k \triangleq [\xi_{k1}, \cdots, \xi_{kN}]^T$ $(k = 1, 2)$, $\bar{p} \triangleq \frac{\sum_{i=1}^N p_i}{N}$, $\bar{q} \triangleq \frac{\sum_{i=1}^N q_i}{N}$, $\bar{r} \triangleq \frac{\sum_{i=1}^N r_i}{N}$, $\delta_1 = [\xi_1 - \bar{p}1_N]$, $\delta_2 = [\xi_2 - \bar{q}1_N]$.

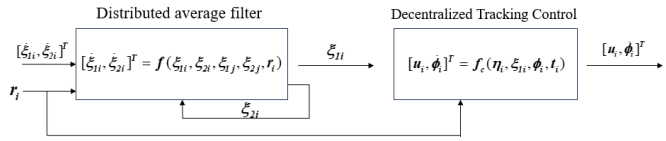

FIGURE 1. Block diagram of the proposed DAT algorithm for agent i. [$N_i :=$ neighbor set of i; $[\xi_{1i}, \xi_{2i}] :=$ filter states; $r_i :=$ reference acceleration of i; $\phi_i :=$ locally updated variable; $f_F, f_T :=$ update laws].

This work is licensed under a Creative Commons Attribution-NonCommercial-NoDerivatives 4.0 License. For more information, see https://creativecommons.org/licenses/by-nc-nd/4

This article has been accepted for publication in IEEE Access. This is the author's version which has not been fully edited and content may change prior to final publication. Citation information: DOI 10.1109/ACCESS.2024.3400623

2) Decentralized Tracking Control Law

The decentralized tracking controller is designed as follow:

$$\begin{aligned} \tau_i &= -\mu_2\phi_i - 2\mu_1\left(\eta_i - \xi_{1i}\right) + r_i \\ \dot{\phi}_i &= -\mu_2\phi_i - \mu_1\left(\eta_i - \xi_{1i}\right) \end{aligned} \tag{6}$$

where ϕ_i is updated locally and $\mu_1, \mu_2 > 0$.

3) Introduction of robustness problem

The controller based on displacement consistency is

$$u = -\bar{L}(\eta - \bar{p}) \tag{7}$$

where u is the control action of USV, and $\bar{L}$ is the Laplacian matrix.

As each USV is equipped with distance sensors and direction sensors, if the scale factor of the distance sensor is different or the direction standard of the direction sensor is not aligned, the actual adjacent position measured by the USV will be inaccurate. It cannot meet the relationship: $\left(x_j - x_i\right)|_{measurement} = aR\left(x_j - x_i\right)|_{actual\ relative\ position}$. Where, a is the distance sensor's scale factor and R is the rotation matrix of the direction sensor. Generally, a and R are the same for each USV.

Let each USV's scale factor a_i $a = \left[a_1 \cdots a_n\right]^T$ and $R = \left[R_1^T \cdots R_n^T\right]^T$ is the stack matrix of the rotation matrix of each USV. Then, defined $D_x = \bar{D}_a D_R$, $a_i > 0$, hence, D_x is always reversible.

Then, we import the scale factor different and misaligned factors into (6) and update the controller as follows:

$$\begin{cases} \tau_i = -\mu_2\phi_i - 2\mu_1\left(D_x\eta_i - \xi_{1i}\right) + r_i \\ \dot{\phi}_i = -\mu_2\phi_i - \mu_1\left(D_x\eta_i - \xi_{1i}\right) \end{cases} \tag{8}$$

E. CONTROL OBJECTIVE

In this paper, our control objective is to design a distributed algorithm for the USVS with double integrator USVs (1), and the time-varying reference given in (2), which each USV has, can achieve the following objectives: $\lim_{t\to\infty}\left|x_i - \frac{\sum_{i=1}^N p_i}{N}\right| = 0$, $\lim_{t\to\infty}\left|v_i - \frac{\sum_{i=1}^N q_i}{N}\right| = 0$

Assumption 1: The difference between their mean $\bar{r} \triangleq \frac{1}{N}\sum_{i=1}^N r$ and each reference acceleration is bounded. Therefore, $\sup_{t\geqslant 0}|r - \bar{r}| \leqslant r_M (0 < r_M < \infty), \forall i = 1, ..., N$.

Assumption 2: The reference input r_i for each USV will become equal when $t \to \infty$. Hence, $\lim_{t\to\infty}|r_i - r_j| = 0, \forall_i, j(i \neq j) = 1, ..., N$.

III. CONTROL DESIGN

In this section, the control scheme is described, and the Lyapunov method is adopted to prove the stability of the control scheme proposed in this paper.

In addition, the DAT algorithm consists of a tracking controller and a distributed filter, which is considered to solve the robust problem of controller. Then, the two parts of the DAT algorithm are introduced in detail.

A. FILTER OF DISTRIBUTED AVERAGING.

Defined the updated law of the filter as follows:

$$\begin{cases} \dot{\xi}_{1i} = \xi_{2i} - k_1 w_i \sum_{j\in N_i} a_{ij}\left(\xi_{1i} - \xi_{1j}\right) \\ \dot{\xi}_{2i} = -k_2 w_i \sum_{j\in N_i} a_{ij}\left(\xi_{2i} - \xi_{2j}\right) + r_i \end{cases} \tag{9}$$

where a_{ij} satisfies $\begin{cases} a_{ij} > 0\ j \in N_i \\ a_{ij} = 0\ j \notin N_i \end{cases}$. ξ_{1i} and ξ_{2i} are the filter states that meets $\xi_{1i}(0) = p_i(0)$ and $\xi_{2i}(0) = q_i(0)$ for any $i \in V$. k_1 and k_2 are control gains. w_i is the ith element of w by offline estimating.

To rewrite equation (9) in the form of a matrix, define the vector in $\mathbb{R}^N$ as follows: $p \triangleq [p_1, \cdots, p_N]^T$, $q \triangleq [q_1, \cdots, q_N]^T$, $r \triangleq [r_1, \cdots, r_N]^T$, $\xi_k \triangleq [\xi_{k1}, \cdots, \xi_{kN}]^T$ $(k = 1, 2)$, $\bar{p} \triangleq \frac{\sum_{i=1}^N p_i}{N}$, $\bar{q} \triangleq \frac{\sum_{i=1}^N q_i}{N}$, $\bar{r} \triangleq \frac{\sum_{i=1}^N r_i}{N}$, $\delta_1 = [\xi_1 - \bar{p}1_N]$, $\delta_2 = [\xi_2 - \bar{q}1_N]$. Where $\bar{p}$, $\bar{q}$ and $\bar{r}$ are the average states.

Then equation (9) is rewritten as follows:

$$\begin{cases} \xi_1 = \xi_2 - k_1 W L \xi_1 \\ \xi_2 = -k_2 W L \xi_2 \end{cases} \tag{10}$$

As $\delta \triangleq \begin{bmatrix} \delta_1^T & \delta_2^T \end{bmatrix}^T \in \mathbb{R}^{2N}$, the following equation can be obtained:

$$\dot{\delta} = A_1\delta + B_1\tilde{r} \tag{11}$$

where $A_1 = \begin{bmatrix} -k_1 W L & I_N \\ \hat{0}_N & -k_2 W L \end{bmatrix}$ and $B_1 = \begin{bmatrix} 0_N \\ I_N \end{bmatrix}$.

Lemma 1: The average of δ_1 and δ_2 are time-invariant under equation (9).

Proof: According to the reference [30], the conclusion of $\bar{\delta}_k(t) := \frac{1_N^T\delta_k(t)}{N} = \frac{1_N^T\delta_k(0)}{N} = 0,\ k = 1, 2$ can be obtained for any $t \geqslant 0$.

B. TRACKING CONTROLLER OF DAT

The tracking controller is designed as follows:

$$\begin{cases} \tau_i = -\mu_2\phi_i - 2\mu_1\left(\eta_i - \xi_{1i}\right) + r_i \\ \dot{\phi}_i = -\mu_2\phi_i - \mu_1\left(\eta_i - \xi_{1i}\right) \end{cases} \tag{12}$$

where $\mu_1, \mu_2 > 0$. ϕ_i is updated locally.

The controller with known dynamics based on displacement consistency is denoted as:

$$u = -\bar{L}(\eta - \bar{p}) \tag{13}$$

where u is the control action of USV, $\bar{L}$ is the Laplacian matrix.

As each USV is equipped with a distance sensor and a direction sensor, if the scale factor of the distance sensor is different and the orientation standard of the direction sensor is not aligned, the actual position measured by the USV is not correctly, which cannot satisfy

$$\left(x_j - x_i\right)|_{measurement} = aR\left(x_j - x_i\right)|_{actual\ relative\ position} \tag{14}$$

This work is licensed under a Creative Commons Attribution-NonCommercial-NoDerivatives 4.0 License. For more information, see https://creativecommons.org/licenses/by-nc-nd/4

This article has been accepted for publication in IEEE Access. This is the author's version which has not been fully edited and content may change prior to final publication. Citation information: DOI 10.1109/ACCESS.2024.3400623

where a is the scale factor of the distance sensor and R is the rotation matrix of the direction sensor, a and R are equal in general.

Define $a = [a_1 ... a_n]^T$ as the scale factor for each USV and $R = \left[R_1^T \cdots R_n^T\right]^T$ as the stacked matrix of the USV's misaligned rotation matrix. Make $D_x = \bar{D}_a D_R$, as $a_i > 0$, D_x is always reversible.

Then, substituting the different scale factor and misaligned factor into equation (12) yields:

$$\begin{cases} \tau_i = -\mu_2 \phi_i - 2\mu_1 \left(D_{\mathrm{x}} \eta_i - \xi_{1i}\right) + r_i \\ \dot{\phi}_i = -\mu_2 \phi_i - \mu_1 \left(D_x \eta_i - \xi_{1i}\right) \end{cases} \tag{15}$$

Define the error variables as:

$$\begin{cases} e_{1i} := x_i - \bar{p} \\ e_{2i} := v_i - \bar{q} \\ e_{3i} := \phi_i \end{cases} \tag{16}$$

Taking the derivative of equation (13) yields:

$$\begin{cases} \dot{e}_{1i} = D_{\mathrm{x}} e_{2i} + D_{\mathrm{x}} \bar{q} - \bar{q} \\ \dot{e}_{2i} = -\mu_2 e_{3i} - 2\mu_1 e_{1i} + 2\mu_1 \delta_{1i} + \tilde{r}_i \\ \dot{e}_{3i} = -\mu_2 e_{3i} - \mu_1 e_{1i} + \mu_1 \delta_{1i} \end{cases} \tag{17}$$

where $\tilde{r}_i := r_i - \bar{r}$, there exist $e_k = [e_{k1}, \cdots, e_{kN}]^T \in R^N$ and $E = \left[e_1^T, e_2^T, e_3^T\right]^T$ for $k = 1, 2, 3$. Then, integrating the equation (17) yields:

$$\dot{E} = A_2 E + B_2 \begin{bmatrix} \delta_1 \\ \tilde{r} \end{bmatrix} + \bar{q} C_2 \tag{18}$$

where

$$A_2 = \begin{bmatrix} 0 & 1 & 0 \\ -2\mu_1 & 0 & -\mu_2 \\ -\mu_1 & 0 & -\mu_2 \end{bmatrix} \otimes I_N$$

$$B_2 = \begin{bmatrix} 0 & 0 \\ 2\mu_1 & 1 \\ \mu_1 & 0 \end{bmatrix} \otimes I_N$$

$$C_2 = \begin{bmatrix} D_x & -1 \\ 0 & 0 \\ 0 & 0 \end{bmatrix} \otimes I_N$$

and $\otimes$ is a Kronecker product.

Make $\tilde{r}$ and δ_1 to be the control input of equation (15), the corresponding input error dynamic can be described as:

$$\begin{cases} \dot{e}_1 = D_{\mathrm{x}} e_2 + D_{\mathrm{x}} \bar{q} - \bar{q} \\ \dot{e}_2 = -\mu_2 e_3 - 2\mu_1 e_1 \\ \dot{e}_3 = -\mu_2 e_3 - \mu_1 e_1 \end{cases} \tag{19}$$

integrating the equation (16) yields:

$$\dot{E} = A_2 E + \bar{q} C_2 \tag{20}$$

Theorem 1: Equation (20) is exponentially stable for $\mu_1, \mu_2 > 0$, therefore, $\begin{bmatrix} e_1^T & e_2^T & e_2^T \end{bmatrix}^T \to 0$ exponentially.

Proof: Select the Lyapunov function as follows:

$$V = \frac{1}{2}\left[e_3^T e_3 + \left(e_2 - e_3\right)^T \left(e_2 - e_3\right) + \mu_1 e_1^T e_1\right] \tag{21}$$

Taking the derivative of the equation (21) yields:

$$\begin{aligned} \dot{V} = &- \mu_2 e_3^T e_3 + \mu_1 \left({D_x}^T - 1\right) e_2^T \left(D_{\mathrm{x}} \eta - \bar{p}\right) + \\ &\mu_1 \left({D_x}^T - 1\right) \bar{q}^T \left(D_{\mathrm{x}} \eta - \bar{p}\right) \end{aligned} \tag{22}$$

Design a new matrix $\breve{M}$, whose elements do not consist of any elements in μ_{ij}. This new matrix assists us in calculating the residual steady-state velocity caused by mismeasurement.

Define $\tilde{\eta}^*$ as the distorted shape and $\tilde{v}^*$ as the residual steady-state velocity, we have:

$$\begin{aligned} &\dot{V} = -\mu_2 e_3^T e_3 + D_{\mathrm{x}} \mu_1 \left({D_x}^T - 1\right) \left(e_2^T + \bar{q}^T\right) \eta - \\ &cr\mu_1 \left({D_x}^T - 1\right) \left(e_2^T + \bar{q}^T\right) \bar{p} + \breve{M}\eta - \breve{M}\eta \\ &= -\mu_2 e_3^T e_3 + \left[D_{\mathrm{x}} \mu_1 \left({D_x}^T - 1\right) \left(e_2^T + \bar{q}^T\right) + \breve{M}\right] \eta - \\ &cr\mu_1 \left({D_x}^T - 1\right) \left(e_2^T + \bar{q}^T\right) \bar{p} - \breve{M}\eta \end{aligned} \tag{23}$$

Ignoring the first term less than 0, corresponding the second and third items to equation (13) yields:

$$\begin{aligned} u = &- \left[D_{\mathrm{x}} \mu_1 \left({D_x}^T - 1\right) \left(e_2^T + \bar{q}^T\right) + \breve{M}\right] \eta \\ &+ \mu_1 \left({D_x}^T - 1\right) \left(e_2^T + \bar{q}^T\right) \bar{p} + \breve{M}\eta \end{aligned} \tag{24}$$

The value of the $\tilde{\eta}^*$, $\tilde{v}^*$ and $\breve{M}$ need to be gained to satisfy the coupling conditions proposed from equation (13) is as follows:

$$\begin{aligned} u = &- \left[D_{\mathrm{x}} \mu_1 \left({D_x}^T - 1\right) \left(e_2^T + \bar{q}^T\right) + \breve{M}\right] \eta \\ &+ \mu_1 \left({D_x}^T - 1\right) \left(e_2^T + \bar{q}^T\right) \bar{p} + \breve{M}\eta \end{aligned} \tag{25}$$

Namely, $u = 0$ and $\dot{V} < 0$ should be achieved. And equation (25) can be transformed into:

$$\begin{aligned} &D_{\mathrm{x}} \mu_1 \left({D_x}^T - 1\right) \left(e_2^T + \bar{q}^T\right) \tilde{\eta}^* - \mu_1 \left({D_x}^T - 1\right) \left(e_2^T + \bar{q}^T\right) \bar{p} \\ &= -1_n \otimes \tilde{v}^* \end{aligned} \tag{26}$$

In the case of $a_i = a^*, R_i = R^*$, we have:

$$\mu_1 \left({D_x}^T - 1\right) \left(e_2^T + \bar{q}^T\right) \left[a^* \left(I_n \otimes R^*\right) \tilde{\eta}^* - \bar{p}\right] = -1_n \otimes \tilde{v}^* \tag{27}$$

where $\tilde{\eta}^* = \frac{1}{a^*}\left(I_n \otimes {R^*}^T\right) \bar{p}$ is satisfied if and only if $\tilde{v}^* = 0$.

If all USVs have the same perception of relative positions, all USVs share the same scale factor a^* and misaligned factor R^* to measure. Then, a distorted but ultimately static shape will be gained:

$$\tilde{\eta}^* = \frac{1}{a^*}\left(I_n \otimes {R^*}^T\right) \bar{p} \tag{28}$$

This work is licensed under a Creative Commons Attribution-NonCommercial-NoDerivatives 4.0 License. For more information, see https://creativecommons.org/licenses/by-nc-nd/4

This article has been accepted for publication in IEEE Access. This is the author's version which has not been fully edited and content may change prior to final publication. Citation information: DOI 10.1109/ACCESS.2024.3400623

Theorem 2: A desired shape consisting of $\bar{p}$ and a framework F, which has a connected graph G without any cycles, is considered. Moreover, the control effect of dynamics (13) is also considered. As the sensing of the USV is precise, namely, $D_x \approx I_{mn}$. In the case of at least 1 USV having a different scale factor and misalignment among all a_i and R_i to measure its available relative position z_{ij}, F can demonstrate a steady-state distorted shape proceeding with residual steady-state velocity $1_n \otimes \tilde{v}^*$.

Proof: Consider the distorted relative position:

$$\begin{aligned}\tilde{\eta}^* = &\left(D_{\mathrm{x}}\mu_1\left({D_x}^T - 1\right)\left(e_2^T + \bar{q}^T\right) + \breve{M}\right)^{-1} \\ &\mu_1\left({D_x}^T - 1\right)\left(e_2^T + \bar{q}^T\right)\bar{p}\end{aligned} \tag{29}$$

where $\tilde{\eta}^* = \bar{p}$ is satisfied if $D_x = I_{mn}$.

Make $\mu_1\left({D_x}^T - 1\right)\left(e_2^T + \bar{q}^T\right) = Q$, therefore:

$$\left[D_{\mathrm{x}}Q\left(D_{\mathrm{x}}Q + \breve{M}\right)^{-1}Q - Q\right]\bar{p} = -1_n \otimes \tilde{v}^* \tag{30}$$

Based on the equations (29), (30) and (25), the following equation can be obtained:

$$\begin{aligned}\breve{M} &= \left(D_{\mathrm{x}}Q + \breve{M}\right)\left[D_{\mathrm{x}}Q\left(D_{\mathrm{x}}Q + \breve{M}\right)^{-1} - 1\right] \\ &= D_{\mathrm{x}}Q - \left(D_{\mathrm{x}}Q + \breve{M}\right)\end{aligned} \tag{31}$$

namely, $\breve{M} = 0$.

Therefore, the coupling condition of equation (25) is satisfied. In equation (24), $u = 0$ can be obtained. Substituting $u = 0$ into equation (22) yields:

$$\dot{V} = -\mu_2 e_3^T e_3 < 0 \tag{32}$$

Equation (32) illustrates that the dynamic error is globally stable when considering the robust problem $E = \begin{bmatrix} {e_1}^T \\ {e_2}^T \\ {e_3}^T \end{bmatrix}$.

Theorem 3: For equation (20) with $\mu_1, \mu_2 > 0$, the following conditions of the tracking error E are satisfied:

1) E is bounded under Assumption 1.
2) E can converge to 0 under Assumption 2.

1) Part 1

In this part, the first condition of Theorem 4 is proved. The solution of equation (17) can be described as:

$$E(t) = e^{A_2(t-\theta_E)}E(\theta_E) + \int_{\theta_E}^{t} e^{A_2(t-\tau)}B_2\begin{bmatrix}\delta_1(\tau) \\ \tilde{r}(\tau)\end{bmatrix}d\tau \tag{33}$$

where $0 \leqslant \theta_E \leqslant t$. Then, based on the reference [27] and equation (19) is globally exponentially stable, the following equation can be obtained:

$$\left\|e^{A_2(t-\theta_E)}\right\|_2 \leqslant v_E e^{-\eta_E(t-\theta_E)} \tag{34}$$

As $v_E, \eta_E > 0$, we can get:

$$\begin{aligned}\|E\|_2 \leqslant &\left(v_E\|E(\theta_E)\|_2\right)e^{-\eta_E(t-\theta_E)} + \\ &\frac{v_E}{\eta_E}\|B_2\|_2 \sup_{\tau\in[\theta_E,t]}\left\|\begin{matrix}\delta_1(t) \\ \tilde{r}(\tau)\end{matrix}\right\|_2\end{aligned} \tag{35}$$

Based on equation (35), we can further get:

$$\|E\|_2 \leqslant \Upsilon_E e^{-\eta_E(t-\theta_E)} + \Psi_E \sup_{t\geqslant 0}\left\|\begin{matrix}\delta_1(t) \\ \tilde{r}(\tau)\end{matrix}\right\|_2 \tag{36}$$

where $\Psi_E := \frac{v_E}{\eta_E}\|B_2\|_2$ and $\Upsilon_E := v_E\|E(\theta_E)\|_2$. $\delta_1(t)$ remains bounded under Assumption 1. Therefore, the equation (36) can be written as:

$$\|E_2\| \leqslant \Upsilon_E + \Psi_E\sqrt{2N}\max\{\delta_{1M}, r_M\} \tag{37}$$

where $\delta_{1M} := \sup_{t\geqslant 0}\|\delta_1\|_2$.

2) Part 2

In this part, the second condition of Theorem 4 is proved.

Make $\sigma_E > 0$ be an arbitrary constant, according to the Assumption 2, we get: $\lim_{t\to\infty}\left\|\begin{matrix}\delta_1(\tau) \\ \tilde{r}(\tau)\end{matrix}\right\|_2 = 0$. Hence, there is $\kappa_{1E} > 0$ such that $\left\|\begin{matrix}\delta_1(\tau) \\ \tilde{r}(\tau)\end{matrix}\right\|_2 \leqslant \frac{\sigma_E}{2\Psi_E}$ for any $t \geqslant \kappa_{1E} > 0$.

From equation (36), the following equation can be obtained:

$\|Et\|_2 \leqslant \Upsilon_E e^{-\eta_E(t-\theta_E)} + \frac{\sigma_E}{2}, \forall t \geqslant \theta_E \geqslant \kappa_{1E}$

When $\lim_{t\to\infty} e^{-\eta_E(t-\theta_E)} = 0$ is satisfied, there exists a $\kappa_{2E} > 0$ such that $e^{-\eta_E(t-\theta_E)} \leqslant \frac{\sigma_E}{2\Upsilon_E}$ for any $t \geqslant \kappa_{2E} > 0$. Hence, there exists $\kappa_E = \max\{\kappa_{1E}, \kappa_{2E}\} > 0$ such that $\|Et\|_2 \leqslant \sigma_E$ for an arbitrary constant σ_E .

As $\lim_{t\to\infty}\left\|\begin{matrix}\delta_1(\tau) \\ \tilde{r}(\tau)\end{matrix}\right\|_2 = 0 \lim_{t\to\infty} e^{-\eta_E(t-\theta_E)} = 0$, when $\kappa_E \to \infty$, there exist $\sigma_E \to 0$. Hence, $E \to 0_{3N}$ is satisfied under Assumption 2.

Therefore, the bounded tracking error under the DAT tracking controller is asymptotic convergence for the convergent acceleration difference.

Therefore, the bounded tracking error under the tracking controller of DAT is asymptotic convergence for the convergent acceleration difference.

IV. SIMULATION

Consider five double integrating USVs as a group, one of the following reference inputs is satisfied:

$$\text{Set 1:}\begin{cases}\bar{p} = \sin\left(\frac{1}{20}t + 0.5\right) \\ \bar{q} = \sin\left(\frac{1}{10}t + 0.5\right)\end{cases}$$

$$\text{Set 2:}\begin{cases}\bar{p} = e^{-0.1t} + \sin\left(\frac{1}{20}t\right) + 0.5 \\ \bar{q} = e^{-0.1t} + \sin\left(\frac{1}{10}t\right) + 0.5\end{cases}$$

The initial parameters for the reference signal and USV state are given in Table 1 and Table 2. The reference input of

This work is licensed under a Creative Commons Attribution-NonCommercial-NoDerivatives 4.0 License. For more information, see https://creativecommons.org/licenses/by-nc-nd/4

This article has been accepted for publication in IEEE Access. This is the author's version which has not been fully edited and content may change prior to final publication. Citation information: DOI 10.1109/ACCESS.2024.3400623

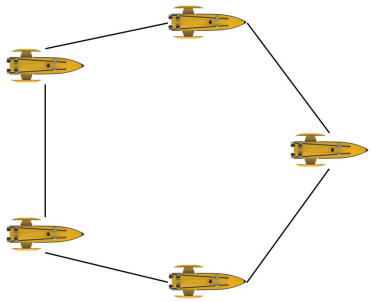

FIGURE 2. Undirected graph.

Set 1 satisfies Assumptions 1, and the reference input of set 2 satisfies Assumptions 2.

Fig. 2 shows the weight-unbalanced strongly connected undirected graph of information flow between USVs. $w = [0.298,\ 0.2649, 0.0795, 0.1589, 0.1987\,]^T$ is determined offline. In addition, w is the left eigenvector of the corresponding φ. Gains of the tracking controller and distributed filter are set as $\mu_1 = 2, \mu_2 = 3, k_1 = 10$, and $k_2 = 20$.

A. SETTINGS

The designed distributed average tracking controller is simulated. Tables 2 and table 3 give the initial parameters for the USV state and reference signal under the first set of reference inputs, and the initial parameters for the USV state and reference signal under the second set of reference inputs are shown in table 4 and table 5. The parameters of USV are shown as follow:

$$m_{11} = 5312200; m_{22} = 8283100; m_{33} = 3745400000;$$
$$m_{23} = 0; m_{32} = 0; d_{11} = 50242; d_{22} = 272290;$$
$$d_{33} = 418940000; d_{23} = -4393300; d_{32} = -4393300;$$

TABLE 1. Weights of USVs.

Parameter	Parameter	Parameter
$a_1 = 0.96843302$	$b_1 = -0.15850664$	$a_{13} = 1$
$a_2 = 1.00873027$	$b_2 = -0.13158391$	$a_{25} = 0.8$
$a_3 = 0.9546316$	$b_3 = -0.07226048$	$a_{34} = 0.5$
$a_4 = 1.04510691$	$b_4 = -0.072021736$	$a_{45} = 0.4$
$a_5 = 1.02358278$	$b_5 = 0.03995607$	$a_{51} = 0.8$

TABLE 2. USVs' states at $t = 0$

USV(i)	1	2	3	4	5
x_i	1.26	-0.80	-0.85	1.39	1.42
y_i	1.07	-1.20	-0.59	1.21	1.47

In order to verify the feasibility of the proposed formation control algorithm, the performance of the formation is tested by using time-varying reference trajectory

TABLE 3. Reference states at $t = 0$

item	parameter
$\bar{P}_i$	0.49
$\bar{q}_i$	0.49

TABLE 4. USVs' states at $t = 0$

USV(i)	1	2	3	4	5
x_i	2.32	-0.23	0.41	1.38	2.29
y_i	2.15	-0.10	0.18	2.33	2.34

TABLE 5. Reference states at $t = 0$

item	parameter
$\bar{P}_i$	1.44
$\bar{q}_i$	1.46

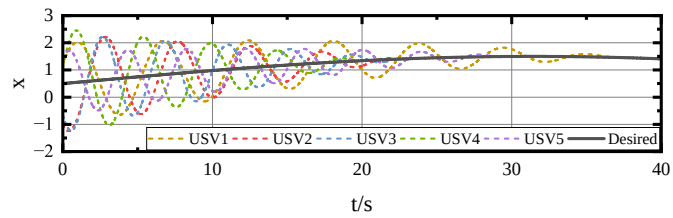

FIGURE 3. Trajectory tracking diagram

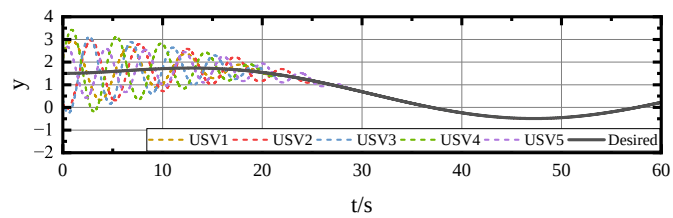

FIGURE 4. Trajectory tracking diagram

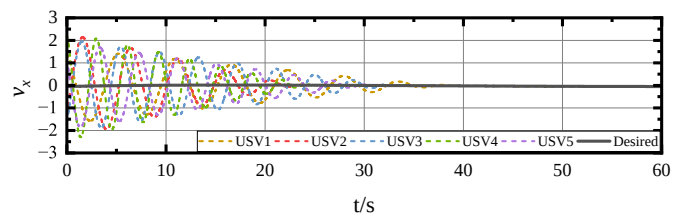

FIGURE 5. Velocity in x direction diagram

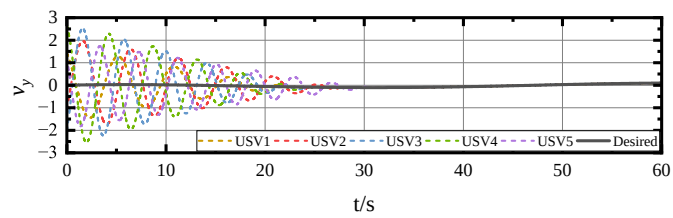

FIGURE 6. Velocity in y direction diagram

This work is licensed under a Creative Commons Attribution-NonCommercial-NoDerivatives 4.0 License. For more information, see https://creativecommons.org/licenses/by-nc-nd/4

This article has been accepted for publication in IEEE Access. This is the author's version which has not been fully edited and content may change prior to final publication. Citation information: DOI 10.1109/ACCESS.2024.3400623

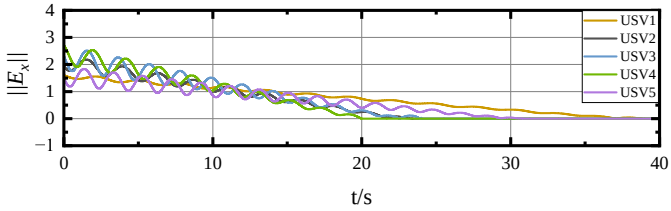

FIGURE 7. Position errors in x direction diagram

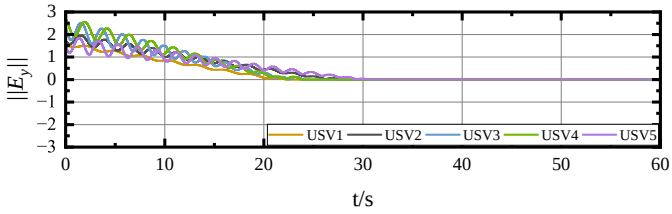

FIGURE 8. Position errors in y direction diagram

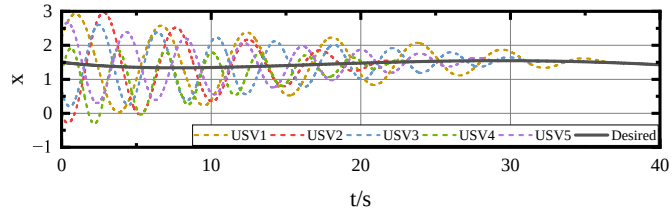

FIGURE 9. Trajectory tracking diagram

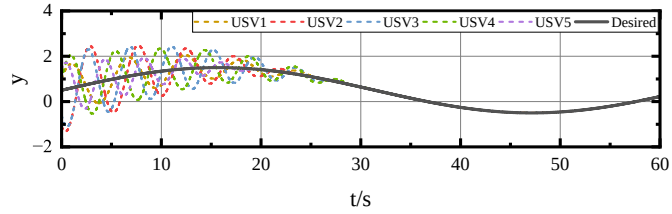

FIGURE 10. Trajectory tracking diagram

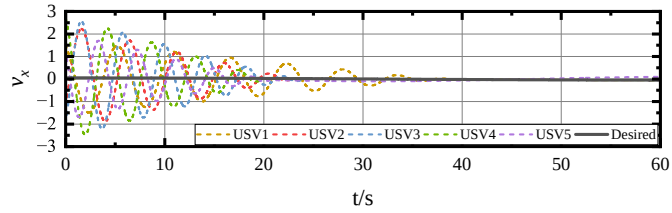

FIGURE 11. Velocity in x direction diagram

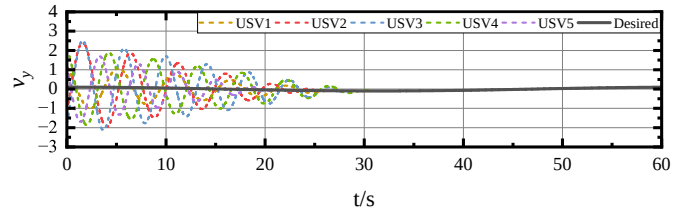

FIGURE 12. Velocity in y direction diagram

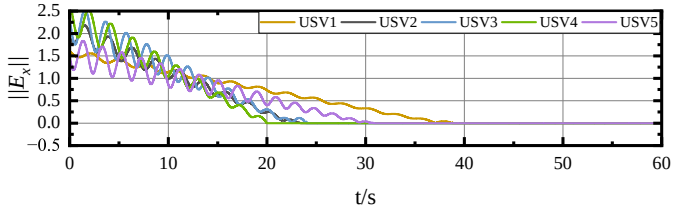

FIGURE 13. Position errors in x direction diagram

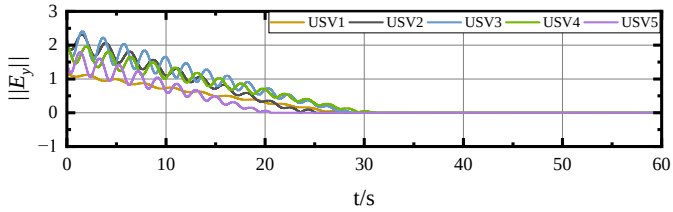

FIGURE 14. Position errors in y direction diagram

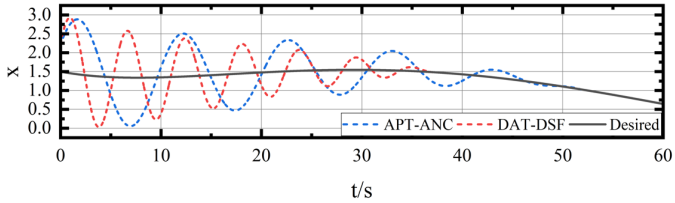

FIGURE 15. Trajectory tracking for USV1

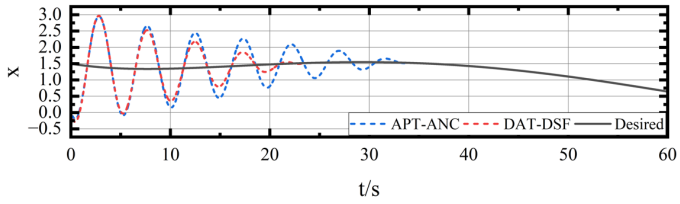

FIGURE 16. Trajectory tracking for USV2

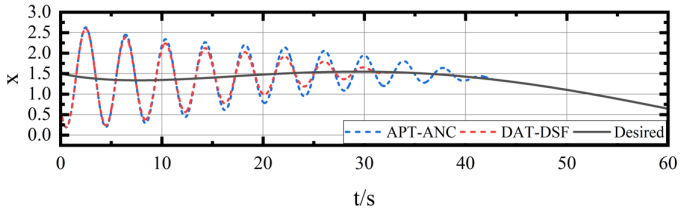

FIGURE 17. Trajectory tracking for USV3

This work is licensed under a Creative Commons Attribution-NonCommercial-NoDerivatives 4.0 License. For more information, see https://creativecommons.org/licenses/by-nc-nd/4

This article has been accepted for publication in IEEE Access. This is the author's version which has not been fully edited and content may change prior to final publication. Citation information: DOI 10.1109/ACCESS.2024.3400623

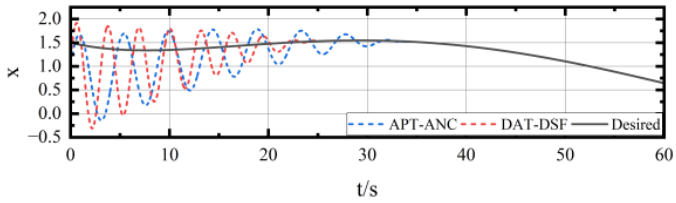

FIGURE 18. Trajectory tracking for USV4

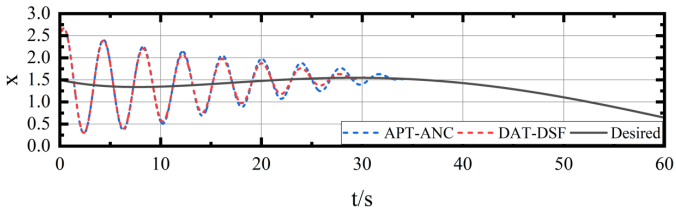

FIGURE 19. Trajectory tracking for USV5

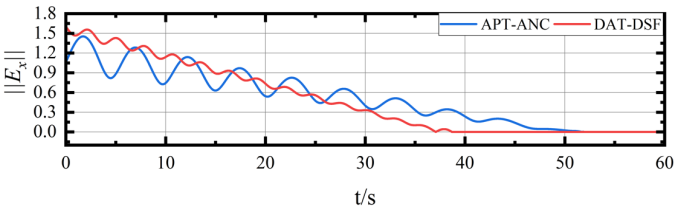

FIGURE 20. Position error for USV1

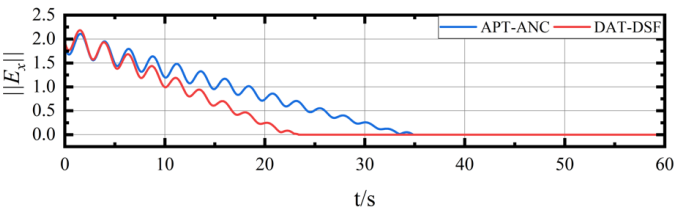

FIGURE 21. Position error for USV2

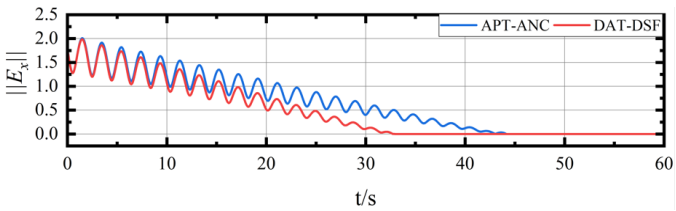

FIGURE 22. Position error for USV3

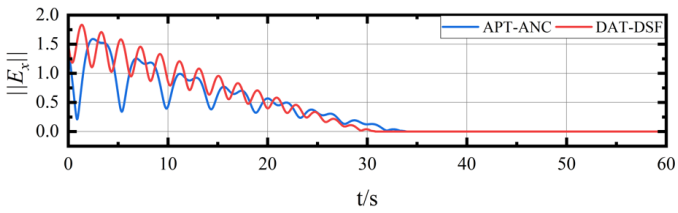

FIGURE 23. Position error for USV4

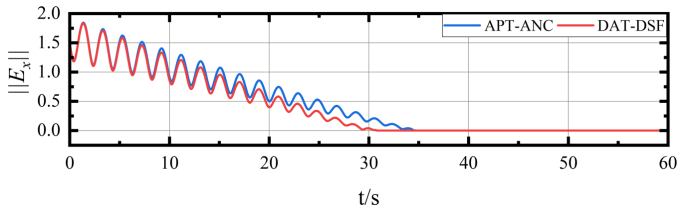

FIGURE 24. Position error for USV5

B. THE SIMULATION RESULTS

Fig. 3 and Fig. 9 show the trajectory diagram of five USVs in the x direction. Fig. 4 and Fig. 10 represent the trajectory tracking of five USVs. Fig. 5 and Fig. 11 show the velocity curve of five USVs in the x direction with time. Corresponding in turn, Fig. 6 and Fig. 12 describes the relationship between velocity and time in the y direction of five USVs. Fig. 7 and Fig. 13 illustrate the position errors of the five USVs in the x direction, respectively. Fig. 8 and Fig. 14 show the position errors of the five USVs in the y direction, respectively. It can be seen from the simulation diagram that under the two sets of reference inputs, the USV can converge in a finite time, and the buffeting is small, which proves the effectiveness of our method.

It is clear from the above figures that both sets of reference inputs guarantee satisfactory control performance in complex real-world environments. The performance of the formation effectively verifies the effectiveness of the distributed average tracking formation scheme. Fig. 3 to Fig. 8 show the relationship between parameters and time under the first group of reference inputs. As shown in Fig. 3, in the beginning, the distribution of the five USVs was disorganized and eventually converged in $t = 36.294s$. In Fig. 4, the five USVs were randomly distributed at the beginning. In the first 30 seconds, the five USVs moved in a certain regularity, and finally at $t = 28.84s$ converged and reached convergence. In Fig. 5 and Fig. 6, the five USVs move forward at different speeds, changing in the velocity interval of $0 - 3m/s$, and finally going stability at $t = 35.72s$ and $t = 29.18s$ respectively. As shown in Figure 7, the initial errors of the five USVs were $1.62, 1.86, 2.26, 2.65$ and 1.36 respectively, which showed a decreasing trend with the increase of time. Finally, at $t = 38.74s$ the errors of the five USVs were all zero, and the formation reached stability. In Fig. 8, the initial error of each USV is above 1, and the fluctuation of the fifth USV is large, the first approach to zero, and the time required for each USV to reach zero error is different, and all errors finally reach zero at $t = 31.05s$. Practice shows that this method improves the stability of formation control and achieves speed convergence in finite time.

Fig. 9 to Fig. 14 show the relationship between parameters and time under the second group of reference inputs. As can be seen from Fig. 9, in the beginning, five USVs were randomly distributed, moved in a particular range along the axis, and finally converged together at $t = 37.59s$; In Fig. 10, at

This work is licensed under a Creative Commons Attribution-NonCommercial-NoDerivatives 4.0 License. For more information, see https://creativecommons.org/licenses/by-nc-nd/4

This article has been accepted for publication in IEEE Access. This is the author's version which has not been fully edited and content may change prior to final publication. Citation information: DOI 10.1109/ACCESS.2024.3400623

the beginning, the five USVs were distributed in a disorderly manner, moving in different directions, their motion tracks were wavy, their motion ranges gradually narrowed, and finally converged together at $t = 28.43s$. As shown in Fig. 11 and Fig. 12, the five USVs begin their movements at different speeds and gradually slow down over time. Ultimately, the velocity is zero respectively at $t = 35.79s$ and $t = 30.18s$, and the formation reaches stability. In Fig. 13, the initial error of the five USVs is between $0.25 - 2.5$, and the mistake on the whole shows a curve reduction with the increase of time, and all the errors drop to zero at the end of $t = 38.99s$. In Fig. 14, the initial errors of the five USVs are all different, and the error fluctuation in the x direction is gentler than that in Fig. 13. Finally, the errors are all reduced to zero at the time of $t = 31.04s$, and the formation reaches stability.

Fig. 15- Fig. 19 show the DAT -based formation control with different scale factor of relative information measurement (DAT-DSF) and the predefined-time adaptive neural tracking control problem for nonlinear multiagent systems (APT-ANC). The blue dotted line is APT-ANC, the red dotted line is DAT-DSF, and the black solid line is the ideal track line. Fig. 15- Fig.19 show the position time diagram of five USVs reaching the ideal state under two different control schemes under the first set of reference inputs.

It can be clearly seen from the figure that both control schemes can achieve satisfactory control performance in complex practical applications. The performance of formation effectively validates the effectiveness of DAT algorithm formation control. As shown in Fig. 15- Fig. 19, we can clearly see that the time taken by the USV controlled by DAT-DSF to reach the desired trajectory is significantly shorter than that of the USV controlled by APT-ANC, which is the case for all five USVs, further demonstrating the effectiveness of the proposed control scheme.

In Fig. 20- Fig. 24, the error comparison of five USVs under two control schemes are shown. The blue solid line is APT-ANC, and the red solid line is DAT-DSF. As shown in Fig. 20, the error of the first USV is small at the beginning under the control of APT-ANC, which fluctuated greatly as time went by, and finally reached the desired position when $t = 51.89s$, and the error approach to 0, while under the control of DAT-DSF, although the error was slightly larger at the beginning, it steadily and rapidly decreased as time went on. When $t = 39.84s$, the desired position is reached and the error approach to 0. As shown in Fig. 21 and Fig. 22, at the beginning ,the error of the USV under the two kinds of control was basically the same, but as time went on, the error of the USV under the control of DAT-DSF significantly decreased, and the reduction rate was significantly decreased, and the reduction rate was significantly faster than that of the USV under the control of APT-ANC, and finally achieved 0 ten seconds ahead of the APT-ANC. This shows that our control scheme can better handle the time-varying external environment, achieve stability in a faster time and have higher control accuracy. Similarly, the same conclusion can be reached under the second set of reference inputs, which we will not cover in detail.

V. CONCLUSION

This paper studies a distributed average tracking (DAT) algorithm based on the relative information to measure the different scale factors of USV formation. The dual integral controller is designed to solve the problem of no velocity so that the USV can reach the expected convergence rate in a limited time when it converges. Based on the dynamic displacement consistency, the controller introduces different scale and misaligned factors and updates the controller to solve the problem of poor robustness of the USV formation. The simulation results show that the control scheme in this paper can solve the problem of stability and robustness of formation control, which proves that the technique has a wide range of practical applications.

REFERENCES

[1] Liu Y, Bucknall R. Path planning algorithm for unmanned surface vehicle formations in a practical maritime environment[J]. Ocean engineering, 2015, 97: 126-144.

[2] Sun X, Wang G, Fan Y, et al. A formation collision avoidance system for unmanned surface vehicles with leader-follower structure[J]. IEEE access, 2019, 7: 24691-24702..

[3] Sun X, Wang G, Fan Y, et al. A formation autonomous navigation system for unmanned surface vehicles with distributed control strategy[J]. IEEE Transactions on Intelligent Transportation Systems, 2020, 22(5): 2834-2845.

[4] Yan R, Pang S, Sun H, et al. Development and missions of unmanned surface vehicle[J]. Journal of Marine Science and Application, 2010, 9: 451-457.

[5] Mu, D.D., Wang, G.F. Fan, Y.S. Formation Control Strategy for Underactuated Unmanned Surface Vehicles Subject to Unknown Dynamics and External Disturbances with Input Saturation. Int. J. Control Autom. Syst. 18, 2742–2752 (2020)

[6] GU N, PENG Z H. Distributed time-varying formation control for unmanned surface vehicles guided by multiple leaders[J]. Chinese Journal of Ship Research, 2020, 15(1): 21-30.

[7] Lv G, Peng Z, Wang H, et al. Extended-state-observer-based distributed model predictive formation control of under-actuated unmanned surface vehicles with collision avoidance[J]. Ocean Engineering, 2021, 238: 109587.

[8] Huang C, Xu H, Batista P, et al. Fixed-time leader-follower formation control of underactuated unmanned surface vehicles with unknown dynamics and ocean disturbances[J]. European Journal of Control, 2023, 70: 100784.

[9] Jin K, Wang J, Wang H, et al. Soft formation control for unmanned surface vehicles under environmental disturbance using multi-task reinforcement learning[J]. Ocean Engineering, 2022, 260: 112035.

[10] Fu, H.; Wang, S.; Ji, Y.; Wang, Y. Formation Control of Unmanned Vessels with Saturation Constraint and Extended State Observation. J. Mar. Sci. Eng. 2021, 9, 772.

[11] L. An, G. -H. Yang, C. Deng and C. Wen. Event-Triggered Reference Governors for Collisions-Free Leader–Following Coordination Under Unreliable Communication Topologies. IEEE Transactions on Automatic Control,2024, 4(69): 2116-2130.

[12] Dong Z, Zhang Z, Qi S, et al. Autonomous Cooperative Formation Control of Underactuated USVs based on Improved MPC in complex ocean environment[J]. Ocean Engineering, 2023, 270: 113633.

[13] He S, Dong C, Dai SL, Adaptive neural formation control for underactuated unmanned surface vehicles with collision and connectivity constraints. Ocean Engineering, 2021,226:108835.

[14] Huang B, Song S, Zhu C, et al. Finite-time distributed formation control for multiple unmanned surface vehicles with input saturation[J]. Ocean Engineering, 2021, 233: 109158.

[15] Dai S L, He S, Lin H, et al. Platoon formation control with prescribed performance guarantees for USVs[J]. IEEE Transactions on Industrial Electronics, 2017, 65(5): 4237-4246.

This work is licensed under a Creative Commons Attribution-NonCommercial-NoDerivatives 4.0 License. For more information, see https://creativecommons.org/licenses/by-nc-nd/4

This article has been accepted for publication in IEEE Access. This is the author's version which has not been fully edited and content may change prior to final publication. Citation information: DOI 10.1109/ACCESS.2024.3400623

[16] Yang S, Pan Y, Cao L, et al. Predefined-Time Fault-Tolerant Consensus Tracking Control for Multi-UAV Systems with Prescribed Performance and Attitude Constraints[J]. IEEE Transactions on Aerospace and Electronic Systems, 2024, 1-14 doi: 10.1109/TAES.2024.3371406.

[17] Pan Y, Ji W, Lam H K, et al. An improved predefined-time adaptive neural control approach for nonlinear multiagent systems[J]. IEEE Transactions on Automation Science and Engineering, 2023, 1-10 doi: 10.1109/TASE.2023.3324397.

[18] Zheng R, Yang R, Lu K, et al. A search and rescue system for maritime personnel in disaster carried on unmanned aerial vehicle[C]//2019 18th International Symposium on Distributed Computing and Applications for Business Engineering and Science (DCABES). IEEE, 2019: 43-47.

[19] Verfuss U K, Aniceto A S, Harris D V, et al. A review of unmanned vehicles for the detection and monitoring of marine fauna[J]. Marine pollution bulletin, 2019, 140: 17-29.

[20] Dobref V, Popa I, Popov P, et al. Unmanned Surface Vessel for Marine Data Acquisition[C]//IOP Conference Series: Earth and Environmental Science. IOP Publishing, 2018, 172: 012034.

[21] Ghapani S, Ren W, Chen F, et al. Distributed average tracking for double-integrator multi-agent systems with reduced requirement on velocity measurements[J]. Automatica, 2017, 81: 1-7.

[22] Liu C L, Shan L, Zhang Y, et al. Hierarchical Average-Tracking Algorithm for Multiagent Systems With Unmatched Constant References Signals[J]. IEEE Transactions on Circuits and Systems II: Express Briefs, 2020, 67(11): 2642-2646.

[23] Dobref V, Popa I, Popov P, et al. Unmanned Surface Vessel for Marine Data Acquisition[C]//IOP Conference Series: Earth and Environmental Science. IOP Publishing, 2018, 172: 012034.

[24] Chen F, Ren W, Lan W, et al. Distributed average tracking for reference signals with bounded accelerations[J]. IEEE Transactions on Automatic Control, 2014, 60(3): 863-869.

[25] Hong H, Wen G, Yu X, et al. Robust distributed average tracking for disturbed second-order multiagent systems[J]. IEEE Transactions on Systems, Man, and Cybernetics: Systems, 2021, 52(5): 3187-3199.

[26] Balestrieri E, Daponte P, De Vito L, et al. Sensors and measurements for unmanned systems: An overview[J]. Sensors, 2021, 21(4): 1518.

[27] Alsos O A, Hodne P, Skåden O K, et al. Maritime autonomous surface ships: Automation transparency for nearby vessels[C]//Journal of Physics: Conference Series. IOP Publishing, 2022, 2311(1): 012027.

[28] Szelangiewicz T, Żelazny K, Antosik A, et al. Application of measurement sensors and navigation devices in experimental research of the computer system for the control of an unmanned ship model[J]. Sensors, 2021, 21(4): 1312.

[29] J. Wang, Y. Xiao, T. Li and C. L. P. Chen. A Jamming Aware Artificial Potential Field Method to Counter GPS Jamming for Unmanned Surface Ship Path Planning. IEEE Systems, 2023,3(17):4555-4566.

[30] Sen A, Sahoo S R, Kothari M. Distributed average tracking with incomplete measurement under a weight-unbalanced digraph[J]. IEEE Transactions on Automatic Control, 2022, 67(11): 6025-6037.

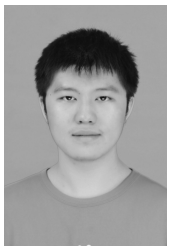

CHENG FU is currently pursuing the B.Eng. degree with the Hubei University of Technology (HBUT), Wuhan. With the help of Dr. Wei Shang, he has completed a few projects in the fields of formation control of unmanned surface vehicle, stability analysis, and visual processing. His research interests include nonlinear control systems and trajectory tracking.

ERHAN WANG is currently pursuing the Bachelor of Engineering degree with the Hubei University of Technology(HBUT),Wuhan. He is also prusuing his research under Dr.Wei Shang. He help complete a few projects in the fields of formation control, stability analysis and trajectory.

XIUCHUAN HUANG (huang020502@163.com) graduated from School of Electrical Engineering, Southwest Jiaotong University and works in Wuhan Railway Vocational College Of Technology. His main research interests are electric traction and drive control, railway traction fault detection and intelligent diagnosis.

QIN YANG is currently pursuing the Bachelor of Engineering degree with the Hubei University of Technology(HBUT),Wuhan. He is also pursuing his research under Dr. Wei Shang. She helped complete lots of jobs of unmanned surface vehicles,which include distributed control, trajectory tracking and formation control.

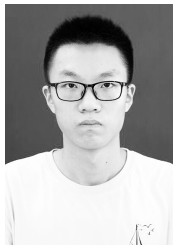

ZHEYU LI is currently pursuing the degree with the Hubei University of Technology(HBUT), Wuhan. He is also pursuing his research under Dr.Wei Shang. He helped complete lots of jobs of unmanned surface vehicles, which include distributed control, formation control and robustness analysis.

WEI SHANG received the Ph.D. degree in aero nautical and astronautical science and technology from the Beijing Institute of Technology, China, in 2017. He is currently a Lecturer with the Hubei University of Technology. His research interests include control theory of multi-agent systems and flight control.

This work is licensed under a Creative Commons Attribution-NonCommercial-NoDerivatives 4.0 License. For more information, see https://creativecommons.org/licenses/by-nc-nd/4